Charged-Higgs-boson production at the LHC: Next-to-leading-order supersymmetric QCD corrections

Stefan Dittmaier, Michael Krämer, Michael Spira, and Manuel Walser

Charged-Higgs-boson production at the LHC:
NLO supersymmetric QCD corrections

STEFAN DITTMAIER

Physikalisches Institut, Albert-Ludwigs-Universität Freiburg,
D–79104 Freiburg, Germany and
Max-Planck-Institut für Physik (Werner-Heisenberg-Institut), Föhringer Ring 6,
D–80805 München, Germany

MICHAEL KRÄMER

Institute for Theoretical Particle Physics and Cosmology, RWTH Aachen University,
D–52056 Aachen, Germany

MICHAEL SPIRA

Paul Scherrer Institut, CH–5232 Villigen PSI, Switzerland

MANUEL WALSER

Paul Scherrer Institut, CH–5232 Villigen PSI, Switzerland and
Institute for Theoretical Physics, ETH Zürich, CH–8093 Zürich, Switzerland

Abstract:

The dominant production process for heavy charged Higgs bosons at the LHC is the associated production with heavy quarks. We have calculated the next-to-leading-order supersymmetric QCD corrections to charged-Higgs production through the parton processes $q\bar{q}, \mathrm{gg} \to \mathrm{tbH}^{\pm}$ and present results for total cross sections and differential distributions. The QCD corrections reduce the renormalization and factorization scale dependence and thus stabilize the theoretical predictions. We present a comparison of the next-to-leading-order results for the inclusive cross section with a calculation based on bottom–gluon fusion $\mathrm{gb} \to \mathrm{tH}^{\pm}$ and discuss the impact of the next-to-leading-order corrections on charged-Higgs searches at the LHC.

1   Introduction

The Higgs mechanism [1] is a cornerstone of the Standard Model (SM) and its supersymmetric extensions. The masses of the fundamental particles, electroweak gauge bosons, leptons, and quarks, are generated by interactions with Higgs fields. The search for Higgs bosons is thus one of the most important tasks for high-energy physics and is being pursued at the upgraded proton–antiproton collider Tevatron with a centre-of-mass (CM) energy of $\sqrt{S} = 1.96$ TeV and at the proton–proton collider LHC, which started operation in 2010 at $\sqrt{S} = 7$ TeV CM energy.

The minimal supersymmetric extension of the Standard Model (MSSM) requires two Higgs doublets leading to five physical scalar Higgs bosons: two (mass-degenerate) charged particles $H^\pm$, one CP-odd neutral particle A, and two CP-even neutral particles h,H. The discovery of a charged Higgs boson, in particular, would provide unambiguous evidence for an extended Higgs sector beyond the Standard Model. Searches at LEP have set a limit $M_{H^\pm} > 79.3$ GeV on the mass of a charged Higgs boson in a general two-Higgs-doublet model [2]. Within the MSSM, the charged-Higgs mass is constrained by the pseudoscalar Higgs mass and the W-boson mass through $M_{H^\pm}^2 = M_A^2 + M_W^2$ at tree level, with only moderate higher-order corrections [3–6]. A mass limit on the MSSM charged Higgs boson can thus be derived from the limit on the pseudoscalar Higgs boson, $M_A > 93.4$ GeV [7], resulting in $M_{H^\pm} \gtrsim 120$ GeV. At the Tevatron, searches for light charged Higgs bosons in top-quark decays $t \to bH^\pm$ [8,9] have placed some constraints on the MSSM parameter space, but do not provide any further generic bounds on $M_H^\pm$.

The LHC will extend the search for charged Higgs bosons to masses up to $M_{H^\pm} \lesssim 600$ GeV [10, 11], where the reach depends in detail on the values of the supersymmetric parameters. In this paper we shall focus on the most promising search channel for heavy $H^\pm$ (with $M_{H^\pm} \gtrsim m_t$) at the LHC, which is the associated production of charged Higgs with heavy quarks,

$$pp \to tbH^\pm + X \,. \tag{1.1}$$

Alternative production mechanisms like quark–antiquark annihilation $q\bar{q}' \to H^\pm$, $H^\pm +$ jet production, associated $H^\pm W^\mp$ production or Higgs pair production have suppressed rates, and it is not yet clear whether a signal could be established in any of those channels (see Ref. [12] and references therein). Some of the above production processes may, however, be enhanced in models with non-minimal flavour violation (see, e.g., Ref. [13]).

Two different formalisms can be employed to calculate the cross section for associated $tbH^\pm$ production. In a four-flavour scheme (4FS) with no b quarks in the initial state, the lowest-order QCD production processes are gluon–gluon fusion and quark–antiquark annihilation, $gg \to tbH^\pm$ and $q\bar{q} \to tbH^\pm$, respectively. The inclusive cross section for $gg \to tbH^\pm$ develops potentially large logarithms $\propto \ln(\mu_F/m_b)$, which arise from the splitting of incoming gluons into nearly collinear $b\bar{b}$ pairs. The large scale μ_F of $\mathcal{O}(M_{H^\pm})$ corresponds to the upper limit of the collinear region up to which factorization is valid. The $\ln(\mu_F/m_b)$ terms can be summed to all orders in perturbation theory by introducing bottom parton densities. This defines the so-called five-flavour scheme (5FS) [14]. The use of bottom distribution functions is based on the approximation that the outgoing b quark is at small transverse momentum and massless, and the virtual b quark is quasi on-shell. In this scheme, the leading-order (LO) process for the inclusive $tbH^\pm$ cross section

is gluon–bottom fusion, gb → tH$^\pm$. The next-to-leading order (NLO) cross section in the 5FS includes $\mathcal{O}(\alpha_\mathrm{s})$ corrections to gb → tH$^\pm$ and the tree-level processes gg → tbH$^\pm$ and $q\bar{q}$ → tbH$^\pm$.

To all orders in perturbation theory the four- and five-flavour schemes are identical, but the way of ordering the perturbative expansion is different, and the results do not match exactly at finite order. For the inclusive production of neutral Higgs bosons with bottom quarks, pp → b$\bar{\text{b}}$H + X, the four- and five-flavour scheme calculations numerically agree within their respective uncertainties, once higher-oder QCD corrections are taken into account [15–18]. However, no NLO comparison of the 4FS and 5FS calculations for charged-Higgs production with heavy quarks exists so far.

There has been considerable progress recently in improving the cross-section predictions for the associated production of charged Higgs bosons with heavy quarks by calculating NLO SUSY-QCD and electroweak corrections in the four and five-flavour schemes [19–26], and the matching of the NLO five-flavour scheme calculation with parton showers [27]. The inclusion of higher-order effects is crucial for an accurate theoretical prediction and, eventually, a determination of Higgs-boson parameters from the comparison of theory and experiment. In this paper we present an independent calculation of the NLO supersymmetric QCD corrections to the process pp → tbH$^\pm$ + X in the 4FS. The calculation within the 4FS allows to describe the dynamics of the final-state bottom quark, which in the 5FS scheme calculation at LO is assumed to be always produced at small transverse momentum and is thus treated inclusively[1]. However, Monte Carlo simulations show that in about 20% of pp → tbH$^\pm$ + X events at the LHC the b quark from the production process has a transverse momentum larger than the b quark from the top-quark decay, and will thus contaminate the event reconstruction [28]. We therefore provide state-of-the art NLO predictions not only for the inclusive cross section but also for various differential distributions. In contrast to previous analyses our results are based on the consistent use of a four-flavour parton distribution function. Furthermore, we present the first comparison of the 4FS and 5FS calculations at NLO for the inclusive tH$^\pm$ cross section.

The paper is organized as follows: In Section 2 we shall describe the calculation of the NLO supersymmetric QCD corrections. Numerical results for MSSM Higgs-boson production at the LHC are presented in Section 3. We conclude in Section 4. The Appendix provides details on the scenario of the supersymmetric model under consideration.

2 Calculation

2.1 LO processes and conventions

In the 4FS the production of charged Higgs bosons in association with top and bottom quarks proceeds at LO through the parton processes [29–31]

$$\text{gg} \rightarrow \text{t}\bar{\text{b}}\text{H}^- \qquad \text{and} \qquad q\bar{q} \rightarrow \text{t}\bar{\text{b}}\text{H}^- \,, \tag{2.1}$$

---

[1]This shortcoming of the 5FS, however, is rectified when going to NLO, where the process gg → tbH$^\pm$ contributes as part of the real corrections.

and the charge-conjugate processes with the $\bar{\text{t}}\text{bH}^+$ final state. Throughout this paper we present results for the $\text{t}\bar{\text{b}}\text{H}^-$ channels, unless stated otherwise. Generic Feynman diagrams that contribute to the LO processes (2.1) are displayed in Fig. 1(a).

In the MSSM, the Yukawa coupling of the charged Higgs boson H^- to a top and bottom quark is given by

$$g_{\text{t}\bar{\text{b}}\text{H}^-} = \sqrt{2}\left(\frac{m_\text{t}}{v}P_R\cot\beta + \frac{m_\text{b}}{v}P_L\tan\beta\right),\tag{2.2}$$

where $v = \sqrt{v_1^2 + v_2^2} = (\sqrt{2}G_\text{F})^{-1/2}$ is the vacuum expectation value of the Higgs field in the Standard Model, and $G_\text{F} = 1.16637 \times 10^{-5}$ GeV^{-2} [32] is the Fermi constant. The ratio of the vacuum expectation values v_1 and v_2 of the two Higgs doublets is denoted by $\tan\beta = v_2/v_1$, and $P_{L/R} = (1 \mp \gamma_5)/2$ are the chirality projectors.

2.2 NLO supersymmetric QCD corrections

The NLO supersymmetric QCD corrections comprise virtual one-loop diagrams, Fig. 1(b,c), gluon radiation processes, Fig. 1(d), and gluon–(anti)quark scattering reactions, Fig. 1(e). The NLO QCD calculation of the SM processes $q\bar{q}, \text{gg} \to Q\overline{Q}\text{H}$, where Q denotes a generic heavy quark, has been described in some detail in Refs. [33, 34] (see also Ref. [35, 36]). Following closely Refs. [33, 34], we have performed two independent calculations of the virtual and real corrections, which are in mutual agreement. A detailed account of one of the two calculations of the virtual corrections is presented in Ref. [37]. In the following we provide a short summary of our methods and mention the tools that have been used.

The Feynman diagrams and amplitudes that contribute to the virtual corrections have been generated with *FeynArts* 1.0 [38] and *FeynArts* 3.2 [39]. The amplitudes have been processed further with two independent in-house *Mathematica* routines, which automatically create output in *Fortran* and *C++*, respectively. The IR (soft and collinear) singularities have been regularized in $D = 4 - 2\epsilon$ dimensions and have been separated analytically from the finite remainder as described in Refs. [34, 40]. This separation also allows for a transparent evaluation of rational terms that result from D-dependent factors multiplying IR divergences appearing as poles in ϵ; in agreement with the general arguments given in Ref. [41] we find that rational terms of IR origin cancel completely. The pentagon tensor integrals have been reduced directly to box integrals following Ref. [42]. This method does not introduce inverse Gram determinants in the reduction process, thereby avoiding numerical instabilities in regions where these determinants become small. Box and lower-point integrals have been reduced to scalar integrals using the standard Passarino–Veltman technique [43]. Sufficient numerical stability is already achieved in this way, but further improvements with the methods of Ref. [44] are in progress. The scalar integrals, finally, have been calculated either analytically or using the results of Refs. [45]. The IR-finite scalar integrals have furthermore been checked with *LoopTools/FF* [46].

Both evaluations of the real-emission corrections employ (independent implementations of) the dipole subtraction formalism [47] for the extraction of IR singularities and for their combination with the virtual corrections. Helicity amplitudes for the real emission processes have been generated and evaluated with *Madgraph* [48] and *HELAS* [49]. The result has been checked by an independent calculation using standard trace techniques.
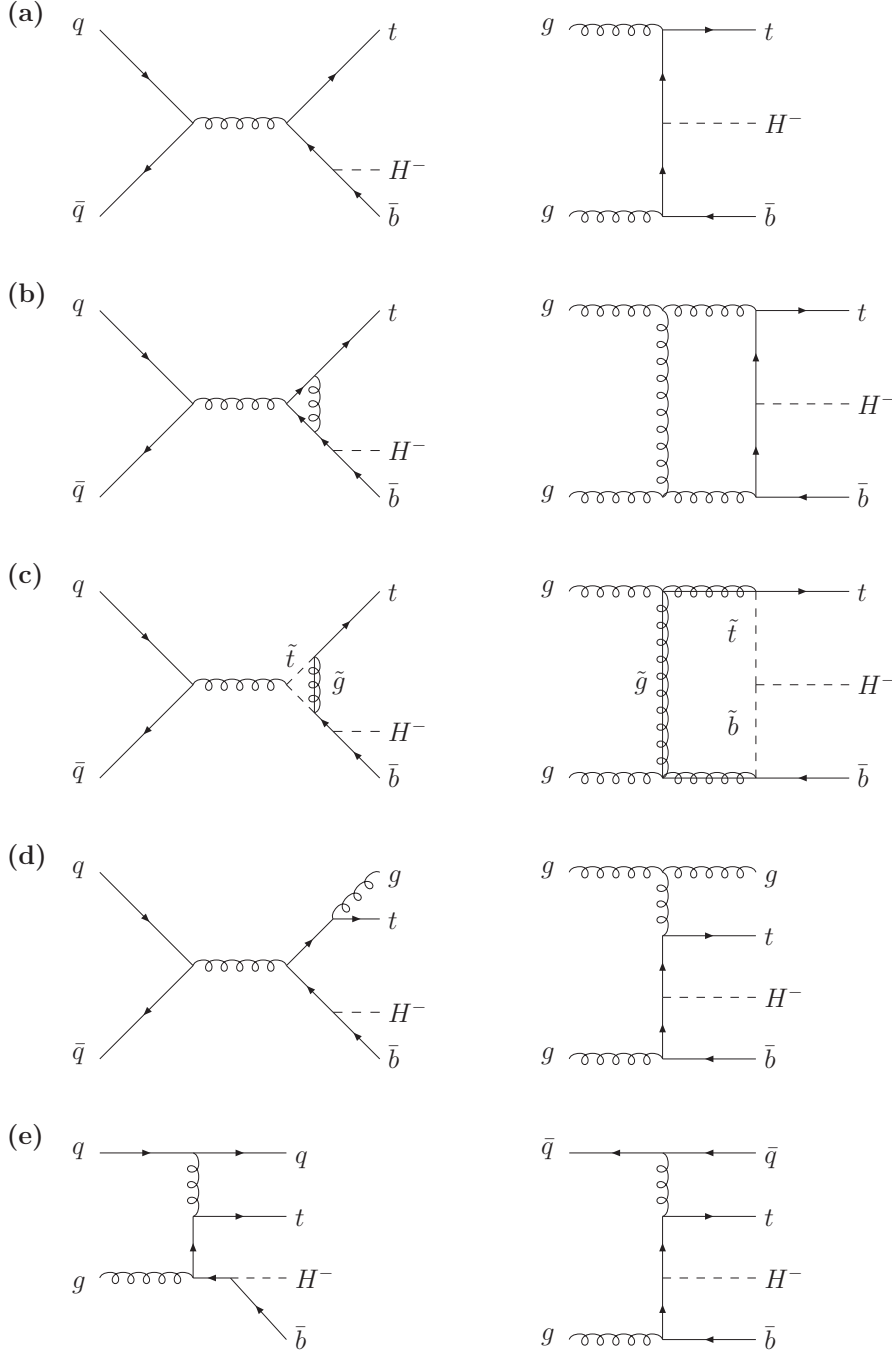
Figure 1: A generic set of diagrams (a) for the Born level, (b) for virtual gluon exchange, (c) virtual gluino and squark exchange, (d) gluon radiation, and (e) gluon–(anti)quark scattering in the subprocesses $q\bar{q}, \mathrm{gg} \to \mathrm{t\bar{b}H^-}$, etc.

2.3 Parameter renormalization and resummation improvements

The renormalization of the strong coupling $\alpha_s(\mu)$ and the factorization of initial-state collinear singularities are performed in the $\overline{\text{MS}}$ scheme. As usual, the top quark and the SUSY particles are decoupled from the running of $\alpha_s(\mu)$. In the 4FS calculation presented here, also the bottom quark is decoupled and the partonic cross section is calculated using a four-flavour α_s. While the top- and bottom-quark masses are defined on-shell, the $\overline{\text{MS}}$ scheme is adopted for the renormalization of the bottom–Higgs Yukawa coupling, which is fixed in terms of the corresponding $\overline{\text{MS}}$ renormalization of the bottom mass. In order to sum large logarithmic corrections $\propto \ln(\mu/m_b)$ we evaluate the Yukawa coupling with the running b-quark mass $\overline{m}_b(\mu)$ [50].

The SUSY loop corrections induce a modification of the tree-level relation between the bottom mass and its Yukawa coupling, which is enhanced at large $\tan\beta$ [51–54]. These corrections can be summed to all orders by the replacement

$$\frac{m_b \tan\beta}{v} \quad \rightarrow \quad \frac{m_b \tan\beta}{v} \frac{(1 - \Delta_b/\tan^2\beta)}{(1 + \Delta_b)} \tag{2.3}$$

in the bottom Yukawa coupling [55, 56], where

$$\Delta_b = \frac{C_F}{2} \frac{\alpha_s}{\pi} m_{\tilde{g}} \mu \tan\beta \, I(m_{\tilde{b}_1}, m_{\tilde{b}_2}, m_{\tilde{g}}), \tag{2.4}$$

with $C_F = 4/3$ and the auxiliary function

$$I(a, b, c) = \frac{1}{(a^2 - b^2)(b^2 - c^2)(a^2 - c^2)} \left(a^2 b^2 \ln \frac{a^2}{b^2} + b^2 c^2 \ln \frac{b^2}{c^2} + c^2 a^2 \ln \frac{c^2}{a^2} \right). \tag{2.5}$$

Here, $\tilde{b}_{1,2}$ are the sbottom mass eigenstates, and $m_{\tilde{g}}$ is the gluino mass. The summation formalism can be extended [56] to include corrections proportional to the trilinear coupling A_b. However, for the MSSM scenarios under consideration in this work, these corrections turn out to be small, and the corresponding summation effects may safely be neglected.

If the LO cross section is expressed in terms of the bottom Yukawa coupling including the summation of the $\tan\beta$-enhanced corrections (2.3), the corresponding NLO contribution has to be subtracted from the one-loop SUSY-QCD calculation to avoid double counting. This subtraction is equivalent to an additional finite renormalization of the bottom mass according to

$$\frac{\delta m_b}{m_b} = \Delta_b \left(1 + \frac{1}{\tan^2\beta} \right). \tag{2.6}$$

As we shall demonstrate in the numerical analysis presented in Section 3, the SUSY-QCD radiative corrections are indeed sizeable at large $\tan\beta$. After summation of the $\tan\beta$-enhanced terms, however, the remaining one-loop SUSY-QCD corrections are very small, below the percent level.

3 Phenomenological analysis

In this section we present NLO SUSY-QCD predictions for the production of heavy charged MSSM Higgs bosons at the LHC. We discuss total cross sections and differential distributions and compare with the 5FS calculations at NLO for the inclusive tH$^-$ cross section.

3.1 Input parameters

Let us first specify the values of the input parameters that enter the numerical analysis. Here, we follow closely the recommendations of the LHC *Higgs Cross Section Working Group* [57].

SM and MSSM masses: The top-quark mass is defined on shell and set to 172.5 GeV [32]. For the bottom pole mass we adopt the value used in the MSTW four-flavour parton distribution function (pdf) [58], i.e. $m_b = 4.75$ GeV, corresponding to a $\overline{\text{MS}}$ mass $\overline{m}_b(\overline{m}_b) = 4.40$ GeV. The bottom pole mass enters the calculation of the matrix elements and the phase space, while the Higgs Yukawa coupling is evaluated using the running bottom mass. As for the MSSM parameters, we will focus on the benchmark scenario SPS 1b [59] which is characterized by a large value of $\tan\beta = 30$ and a correspondingly large associated production cross section $pp \to tbH^{\pm} + X$ at the LHC. The SPS 1b input parameters are specified in Appendix A. The MSSM tree-level relations are used to determine the squark masses that enter the SUSY-QCD corrections. The charged-Higgs mass is calculated from $\tan\beta$ and the mass of the pseudoscalar Higgs, M_A, taking into account higher-order corrections up to two loops in the effective potential approach [60,61] as included in the program *HDECAY* [62]. For the Higgs mass determination we use a five-flavour α_s with $\alpha_s(M_Z) = 0.120$ [63]. The top quark, the squarks, and the gluino are always decoupled from the running of the strong coupling.

Higgs Yukawa coupling: The evaluation of the bottom–Higgs Yukawa coupling, which involves the running b-quark mass and the summation of the $\tan\beta$-enhanced SUSY-QCD corrections through Δ_b, is also based on a five-flavour α_s with $\alpha_s(M_Z) = 0.120$. Our default choice for the renormalization scale that enters the calculation of the running b-quark mass is the average mass of the final-state particles, $\mu = (m_t + m_b + M_{H^-})/3$. The scale of α_s in the summation factor of the Yukawa coupling (cf. Eq. (2.4)), on the other hand, is determined by the masses of the supersymmetric particles in the loop and is chosen as $\mu = (m_{\tilde{b}_1} + m_{\tilde{b}_2} + m_{\tilde{g}})/3$. This scale choice for the effective short-distance contributions included in the resummed bottom Yukawa coupling is justified by the recent NNLO results for the Δ_b corrections [64].

Hadronic cross section: Our cross-section calculation is defined in the four-flavour scheme, i.e. with no b quarks in the initial state. Thus, for a consistent evaluation of the hadronic cross sections we adopt the recent MSTW four-flavour pdf [58]. The partonic cross section is calculated using the corresponding four-flavour α_s with $\Lambda^{(4)} = 0.371$ GeV ($\alpha_s(M_Z) = 0.1149$) at NLO, except for the Higgs Yukawa coupling which is evaluated with a five-flavour α_s as explained above. Our default choice for the renormalization and factorization scales that enter the partonic cross section and the pdf is $\mu = (m_t + m_b + M_{H^-})/3$. Note that the LO cross-section predictions have been obtained by using the corresponding LO four-flavour pdf set [58], a LO α_s with $\Lambda^{(4)} = 0.322$ GeV ($\alpha_s(M_Z) = 0.13355$) for the partonic cross section, and a LO running b-quark mass using a LO five-flavour α_s with $\alpha_s(M_Z) = 0.139$ [63].

3.2 Total cross section and scale dependence

We first discuss the scale dependence of the total $pp \to t\bar{b}H^- + X$ cross section at the LHC, both for the current CM energy $\sqrt{S} = 7$ TeV and for the LHC design energy of $\sqrt{S} = 14$ TeV. Note that in NLO QCD the cross section for the charge-conjugate process $pp \to \bar{t}bH^+ + X$ at the LHC is identical to $pp \to t\bar{b}H^- + X$ and can be included by multiplying the results presented below by a factor of two. The renormalization and factorization scales that enter the hadronic cross section and the running b-quark mass are identified and varied around the central value $\mu_0 = (m_t + m_b + M_{H^-})/3$, the scale of α_s in the summation factor of the Yukawa coupling (cf. Eq. (2.4)), on the other hand, is kept fixed. Figure 2 shows the scale dependence of the LO and complete NLO SUSY-QCD cross sections at the LHC with 7 and 14 TeV energy, for the SPS 1b benchmark point and $M_A = 200$ GeV, corresponding to $M_{H^\pm} = 214.27$ GeV. As anticipated, the scale dependence of the theoretical prediction is significantly reduced at NLO, with a remaining uncertainty of approximately $\pm 25\%$ when μ is varied between $\mu_0/3$ and $3\mu_0$, compared to approximately $\pm 100\%$ at LO. At the central scale, the K-factor, $K = \sigma_{NLO}/\sigma_{LO}$ is close to one for both CM energies. Note, however, that the K-factor strongly depends on the definition of the LO cross section. As described above, our LO cross section prediction includes the summation of a certain class of QCD corrections through a running Yukawa coupling, and has been evaluated using a LO pdf and α_s. We also find a significant reduction of the spurious scale dependence at NLO for the exclusive cross section, where the b quark is required to be produced with $p_{T,b} > 20$ GeV, see Figure 3. The QCD corrections for the exclusive cross section are moderate and negative at the central scale, with a corresponding K-factor of $K \approx 0.85$.

The total LO and NLO SUSY-QCD cross sections for $pp \to t\bar{b}H^- + X$ at the LHC with 7 and 14 TeV are shown in Figure 4 as a function of the Higgs-boson mass. Note that $t\bar{b}H^-$ production at the LHC is dominated by gluon-induced processes which provide more than 95% of the cross section. The K-factor is displayed in the lower part of the plots, together with the scale dependence of the LO and NLO predictions. We observe that for our choice of the central scale, $\mu_0 = (m_t + m_b + M_{H^-})/3$, the K-factor is moderate over the whole range of Higgs-boson masses. Furthermore, the scale dependence is reduced at NLO also for large Higgs masses, indicating that the perturbative expansion is well under control. Representative values for the total cross section at 14 TeV are listed in Table 1. To facilitate the comparison with other calculations we also show in Table 1 the running b-quark mass, which enters the Higgs Yukawa coupling and thus strongly affects the overall normalization of the cross section. Requiring the bottom quark to be produced with $p_{T,b} > 20$ GeV reduces the inclusive cross section by approximately 60%, see Figure 5. We note that our numerical results for the exclusive cross section with $p_{T,b} > 20$ GeV and $|\eta_b| < 2.5$ do not agree with those presented in Ref. [24]. The cross section predictions in Ref. [24] are a factor 2–3 smaller than ours.

If we adopt – inconsistently – the five-flavour MSTW pdf [63], on which the four-flavour set is based, the cross section decreases by approximately 10%: gluon splitting into bottom-quark pairs is included in the evolution of the five-flavour pdf and depletes the gluon flux compared to the four-flavour pdf. Note that the recent fixed-flavour parton densities of Ref. [65] are based on three active flavours in the proton and five active flavours

M_A [GeV]	$M_{H^\pm}$ [GeV]	$\overline{m}_b^{\mathrm{NLO}}(\mu)$ [GeV]	$\sigma(\mathrm{pp} \to \bar{t}bH^- + X)$ [fb]		$K = \sigma_{\mathrm{NLO}}/\sigma_{\mathrm{LO}}$
			LO	NLO	
200	214.27	2.91	609	599(2)	0.98
300	309.69	2.86	257	263(1)	1.02
400	407.32	2.82	118	124(1)	1.05
500	505.88	2.79	58.4	62.5(2)	1.07

Table 1: Total cross sections and K-factors for pp $\to$ t$\bar{b}$H$^-$ + X at the LHC (14 TeV). The renormalization and factorization scales are set to $\mu = (m_t + m_b + M_{H^-})/3$. The error from the Monte Carlo integration on the last digit is given in parenthesis if significant. The MSTW four-flavour pdf [58] is adopted. In the third column we show the running b-quark mass evaluated at the default renormalization scale.

in the evolution of α_s; we can thus not use the pdf set of Ref. [65] without modification of our calculation.

In Table 2 we show the individual contributions to the NLO cross section due to the Standard Model QCD corrections and the genuine SUSY-QCD effects, split further into the impact of the $\tan\beta$-enhanced corrections included in the summation factor Δ_b and the remainder of the genuine SUSY contributions. The cross section labeled σ_0 denotes the LO parton cross section evaluated with NLO running b-quark mass, pdf and α_s. The NLO Standard Model QCD corrections, δ_{QCD}, increase the prediction by approximately 60%, nearly independent of the value of the Higgs-boson mass. This increase is partially compensated by the $\tan\beta$-enhanced SUSY corrections, $\delta_{\mathrm{SUSY}}^{\tan\beta-\mathrm{resum.}}$, which amount to approximately -30%. The impact of the remaining one-loop SUSY-QCD corrections, $\delta_{\mathrm{SUSY}}^{\mathrm{remainder}}$, is marginal, below the percent level. We also show the result of a fixed-order SUSY-QCD calculation, $\sigma_{\mathrm{NLO}}^{\mathrm{fixed-order}}$, which does not include the $\tan\beta$-enhanced corrections beyond NLO. We find that the effect of the $\tan\beta$-summation beyond NLO, included in our best cross-section prediction σ_{NLO}, is moderate, at the level of 10%.

Supersymmetric electroweak $\mathcal{O}(\alpha)$ corrections have been studied in Ref. [25] for charged Higgs production in the five-flavour scheme, and in Ref. [66] for the related process of neutral MSSM Higgs production in bottom-quark fusion. It has been shown in [66] that the leading electroweak corrections can be taken into account by an appropriate definition of the couplings and the running b-mass in an improved Born approximation. The remaining non-universal corrections have been found to be small, typically of the order of a few percent. It would be interesting to see whether similar conclusions also hold for the process of charged-Higgs production in the four-flavour scheme studied here.

$M_{\mathrm{H}^\pm}$ [GeV]	$\sigma_{\mathrm{NLO}} = \sigma_0 \times (1+\delta_{\mathrm{SUSY}}^{\tan\beta-\mathrm{resum.}}) \times (1+\delta_{\mathrm{QCD}}+\delta_{\mathrm{SUSY}}^{\mathrm{remainder}})$				$\sigma_{\mathrm{NLO}}^{\mathrm{fixed-order}}$ [fb]
	σ_0 [fb]	δ_{QCD}	$\delta_{\mathrm{SUSY}}^{\tan\beta-\mathrm{resum.}}$	$\delta_{\mathrm{SUSY}}^{\mathrm{remainder}}$	
214.27	544	0.56	-0.31	-0.0015	596(2)
309.69	234	0.61	-0.31	-0.0021	268(1)
407.32	109	0.63	-0.31	-0.0017	129(1)
505.88	54.1	0.63	-0.31	-0.0008	65.1(2)

Table 2: LO total cross section σ_0 and NLO corrections δ relative to σ_0 for pp $\to$ t$\bar{\mathrm{b}}$H$^-$ + X at the LHC (14 TeV). The error from the Monte Carlo integration on the last digit is given in parenthesis if significant. The MSTW pdf [58] is adopted and the renormalization and factorization scales have been set to $\mu = (m_{\mathrm{t}} + m_{\mathrm{b}} + M_{\mathrm{H}^-})/3$. "QCD" denotes the NLO QCD corrections only, "SUSY/$\tan\beta$–resum." the $\tan\beta$-enhanced SUSY corrections, "SUSY/remainder" the remaining one-loop SUSY corrections and "NLO/fixed-order" the complete NLO calculation without summation of the $\tan\beta$-enhanced terms.

3.3 Differential distributions

Let us now turn to the transverse-momentum and rapidity distributions of the final-state particles shown in Figure 6. The distributions have been evaluated for the default scale choice $\mu = (m_{\mathrm{t}} + m_{\mathrm{b}} + M_{\mathrm{H}^-})/3$. The p_{T}-distributions of the top quark and the Higgs boson are rather similar, with a maximum at $p_{\mathrm{T}} \approx 100$ GeV. The transverse-momentum distribution of the bottom quark is much softer with $\sigma_{\mathrm{NLO}}(p_{\mathrm{T,b}} < 25 \text{ GeV})/\sigma_{\mathrm{NLO}} \approx 0.7$. The heavy particles, i.e. the top quark and the Higgs boson, are preferentially produced at central rapidities with $|y| \lesssim 2.5$, while the rapidity distribution of the bottom quark is rather flat in the region $|y| \lesssim 4$.

The impact of the higher-order corrections on the shape of the Higgs, top- and bottom-quark transverse-momentum and rapidity distributions is shown in Figures 7, 8, and 9, respectively. The lower part of each plot shows the K-factor. We find that the shape of the top and Higgs transverse-momentum distribution is not strongly affected by the higher-order corrections in the range of p_{T} relevant for the experimental analysis. On the other hand, the bottom quark p_{T}-distribution, which extends to $p_{\mathrm{T,b}} \gg m_{\mathrm{b}}$, is softened at NLO, with the K-factor decreasing from K = 1.1 at $p_{\mathrm{T,b}} \approx 20$ GeV to K = 0.5 at $p_{\mathrm{T,b}} \approx 300$ GeV. The large impact on the $p_{\mathrm{T,b}}$ distribution is due to collinear gluon radiation off bottom quarks that is enhanced by a factor $\alpha_{\mathrm{s}} \ln(m_{\mathrm{b}}/p_{\mathrm{T,b}})$. The enhancement should be significantly reduced if the bottom quarks are reconstructed from jets, since the application of a jet algorithm treats the bottom–gluon system inclusively in the collinear cone, so that the logarithmic enhancement cancels out. The NLO corrections do not significantly change the shape of the rapidity distributions.

We have also evaluated the differential distributions with the renormalization and factorization scales set to the average transverse mass, $\mu = (m_{\mathrm{T,b}} + m_{\mathrm{T,t}} + m_{\mathrm{T,H}})/3$,

where $m_{\mathrm{T,b}} = \sqrt{m_{\mathrm{b}}^2 + p_{\mathrm{T,b}}^2}$, etc. We find that the shapes of the NLO distributions are not significantly affected by such a change. The LO transverse-momentum distributions, however, do provide a better description of the NLO shapes when evaluated with $\mu = (m_{\mathrm{T,b}} + m_{\mathrm{T,t}} + m_{\mathrm{T,H}})/3$.

3.4   Comparison with the 5FS calculation

As discussed in Section 1, in the 5FS the LO process for the inclusive $\mathrm{tH}^{\pm}$ cross section is gluon–bottom fusion, $\mathrm{gb} \to \mathrm{tH}^{\pm}$. The NLO cross section includes $\mathcal{O}(\alpha_{\mathrm{s}})$ corrections to $\mathrm{gb} \to \mathrm{tH}^{\pm}$ and the tree-level processes $\mathrm{gg} \to \mathrm{tbH}^{\pm}$ and $q\bar{q} \to \mathrm{tbH}^{\pm}$, and has been calculated in Refs. [21, 22, 27]. In Figure 10 we present a comparison of the 4FS and 5FS calculations at NLO QCD for the inclusive $\mathrm{pp} \to \mathrm{tH}^- + X$ cross section at the LHC. The 5FS calculation is taken from Ref. [21] and is evaluated with the five-flavour MSTW pdf [63] and the set of input parameters described above. In particular, the renormalization and factorization scales have been set to $\mu_0 = (m_{\mathrm{t}} + m_{\mathrm{b}} + M_{\mathrm{H}^-})/3$, as in the 4FS calculation. The error band indicates the theoretical uncertainty when the renormalization and factorization scales are varied between $\mu_0/3$ and $3\mu_0$. Thus, the error band also includes the scale choice $\mu_{\mathrm{F}} = (m_{\mathrm{t}} + M_{\mathrm{H}^-})/5$ for the 5FS calculation advocated in Refs. [21, 22]. The cross sections shown in Figure 10 do not include the NLO SUSY effects, which can be incorporated within good precision by simply adjusting the bottom Yukawa coupling according to Eq. (2.3). Taking the scale uncertainty into account, the 4FS and 5FS cross sections at NLO are consistent, even though the predictions in the 5FS at our choice of the central scale are larger than those of the 4FS by approximately 25%, rather independent of the Higgs-boson mass. Qualitatively similar results have been obtained from a comparison of 4FS and 5FS NLO calculations for single-top production at the LHC [67]. Note that the bottom pdf of the recent five-flavour MSTW fit [63] is considerably smaller than that of previous fits [68] and has lead to a significant decrease in the 5FS cross section prediction.

3.5   Discovery reach

Accurate theoretical predictions for the charged-Higgs production cross section are crucial to exploit the LHC potential for MSSM Higgs-boson searches. To exemplify the importance of reducing the theoretical uncertainty through NLO calculations, we consider the discovery reach in the search channel $\mathrm{pp} \to \mathrm{tbH}^{\pm} + X$ followed by the hadronic decay $\mathrm{H}^{\pm} \to \tau^{\pm} \nu_{\tau}$ with $\tau \to \mathrm{hadrons} + \nu_{\tau}$, as analyzed for the CMS detector in Refs. [28, 69]. The number of signal events is given by

$$N_{\mathrm{signal}} = \int\!\mathcal{L} \times \sigma(\mathrm{pp} \to \mathrm{tbH}^{\pm} + X) \times \mathrm{BR}(\mathrm{H}^{\pm} \to \tau^{\pm}\nu_{\tau}) \times \mathrm{BR}(\tau \to \mathrm{hadrons}) \times \mathrm{exp.\ efficiency}\,, \tag{3.1}$$

where $\int\!\mathcal{L}$ denotes the collider luminosity. The experimental efficiency has been determined in Ref. [28] as a function of the Higgs-boson mass:

$M_{\mathrm{H}^{\pm}}$ [GeV]	171.6	180.4	201.0	300.9	400.7	600.8
exp. eff. $[10^{-4}]$	3.5	4.9	5.0	23	32	42

.

The QCD background processes lead to 1.7 ± 1 events after cuts, independent of $M_{\mathrm{H}^\pm}$, so that 14 or more signal events are needed for a $5\,\sigma$ discovery [28]. We determine the number of signal events from Eq. (3.1) for the benchmark scenario SPS 1b, varying $\tan\beta$ and M_A while keeping all other supersymmetric parameters fixed. The branching ratio $\mathrm{BR}(\mathrm{H}^\pm \to \tau^\pm \nu_\tau)$ varies strongly with M_A and has been calculated with *SUSY-Hit* [70]. The branching ratio of the hadronic τ decay has been set to $\mathrm{BR}(\tau \to \mathrm{hadrons}) = 0.65$ [32], and we assume an integrated luminosity of $\int \mathcal{L} = 30$ fb^{-1}. In Figure 11 we show the $5\,\sigma$ discovery contours for $\mathrm{H}^\pm$ as a function of $\tan\beta$ and $M_{\mathrm{H}^\pm}$, where the number of signal events in Eq. (3.1) has been evaluated using the LO and NLO 4FS calculation presented in this paper. We show results for the central scale $\mu_0 = (m_\mathrm{t} + m_\mathrm{b} + M_{\mathrm{H}^-})/3$ and results for the renormalization and factorization scales set to $\mu = \mu_0/3$ and $3\mu_0$, respectively. Higgs-boson discovery is possible in the areas above the curves shown in the figure. Figure 11 demonstrates that the reduction of the scale uncertainty is crucial to exploit the potential of the LHC for charged Higgs-boson discovery. Note that a more detailed study of the supersymmetric parameter dependence of the discovery contours is presented in Ref. [69]. The importance of a reduced scale dependence through the calculation of higher-order corrections for charged-Higgs-boson discovery, however, is generic and largely independent of the supersymmetric scenario considered.

4 Conclusions

We have presented the next-to-leading order supersymmetric QCD corrections to charged-Higgs-boson production at the LHC in the four-flavour scheme through the parton processes $q\bar{q}, \mathrm{gg} \to \mathrm{tbH}^\pm$. While the K-factor is moderate at the central scale $\mu = (m_\mathrm{t} + m_\mathrm{b} + M_{\mathrm{H}^-})/3$, the QCD corrections considerably reduce the renormalization and factorization scale dependence and thus stabilize the theoretical predictions. We find that the shapes of the top-quark and Higgs transverse-momentum distributions are not strongly affected by the higher-order corrections. On the other hand, the bottom-quark p_T-distribution is softened at NLO, depending in detail on the reconstruction method of the bottom quarks. The NLO corrections do not significantly change the shape of the rapidity distributions. We have presented a first comparison of the four-flavour scheme NLO inclusive cross sections with a five-flavour scheme calculation based on bottom–gluon fusion. The results of the two schemes are consistent within the scale uncertainties, with the central predictions in the five-flavour scheme being larger than those of the four-flavour scheme by approximately 25%. Finally, by referring to a recent CMS study [28] we have demonstrated that NLO predictions for the charged-Higgs production cross section are crucial to exploit the LHC potential for MSSM Higgs-boson searches.

Acknowledgments

Figure 2: Variation of the LO and NLO cross sections with the renormalization and factorization scales for pp → t$\bar{\text{b}}$H$^-$ + X at the LHC (7 and 14 TeV).
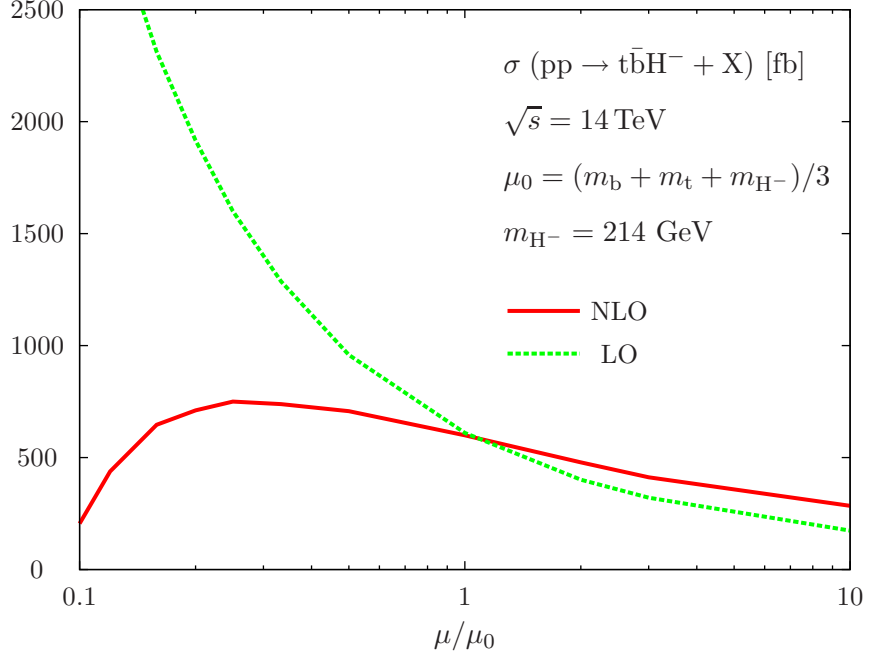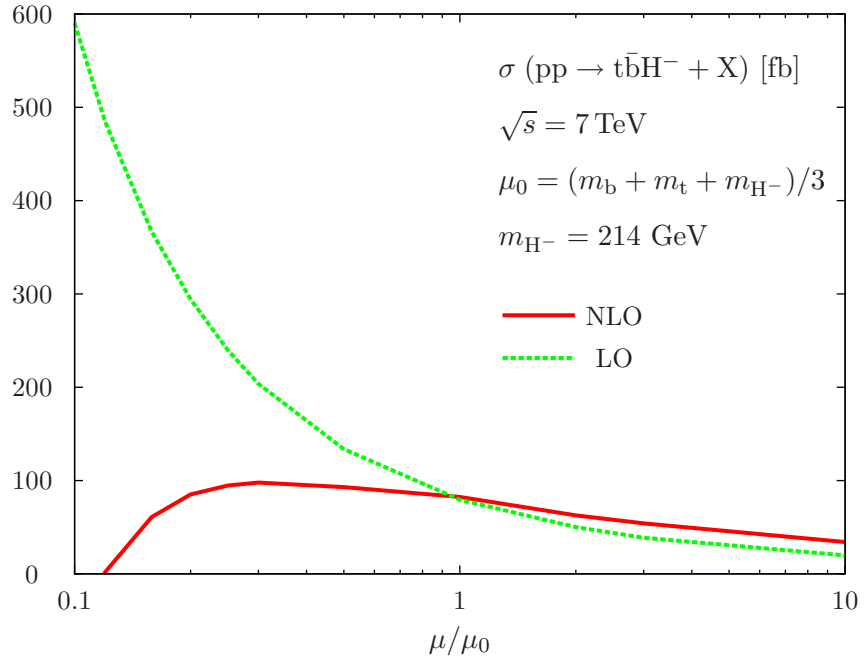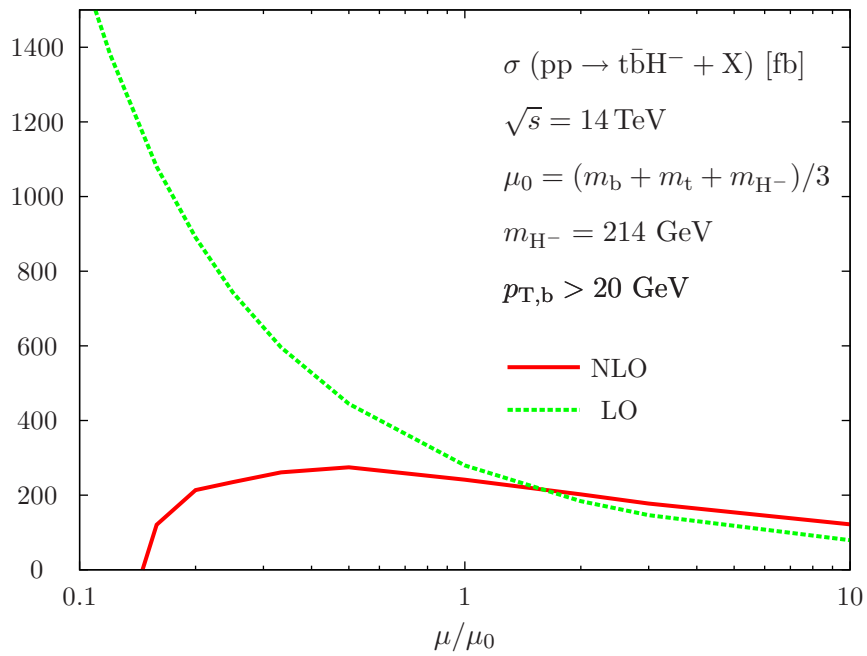
Figure 3: Variation of the LO and NLO cross sections with the renormalization and factorization scales for $pp \rightarrow t\bar{b}H^- + X$ at the LHC (14 TeV), with a cut of $p_{T,b} > 20$ GeV on the b-quark transverse momentum.
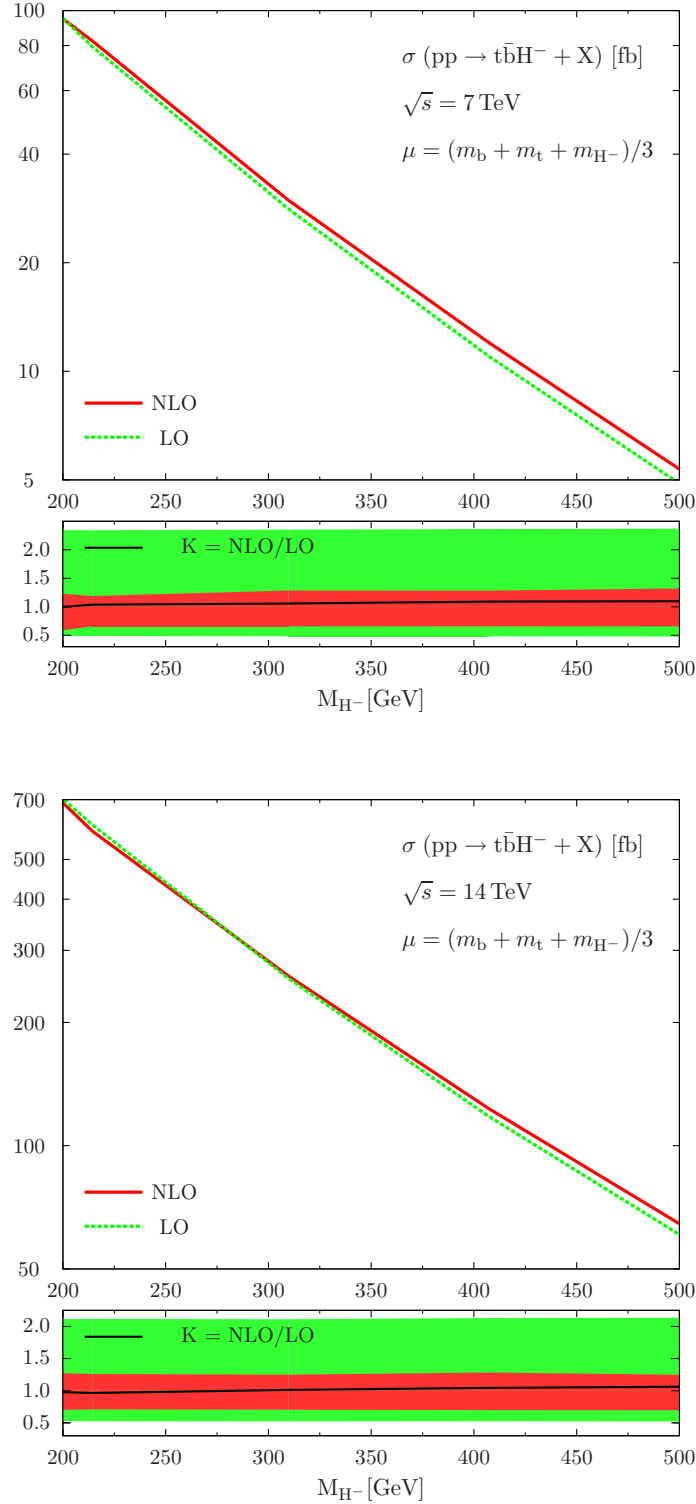
Figure 4: Total LO and NLO cross sections for pp $\rightarrow$ t$\bar{\text{b}}$H$^-$ + X at the LHC (7 TeV and 14 TeV) as a function of the Higgs-boson mass. The lower plots show the K-factor, K = $\sigma_{\text{NLO}}/\sigma_{\text{LO}}$, and the scale dependence of the LO and NLO cross section predictions for $\mu_0/3 < \mu < 3\mu_0$.
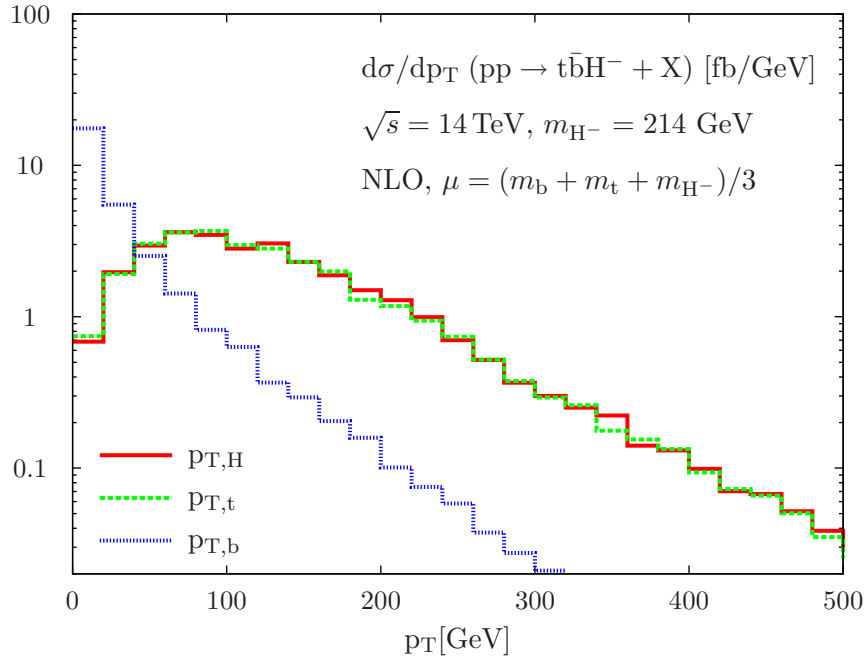
15
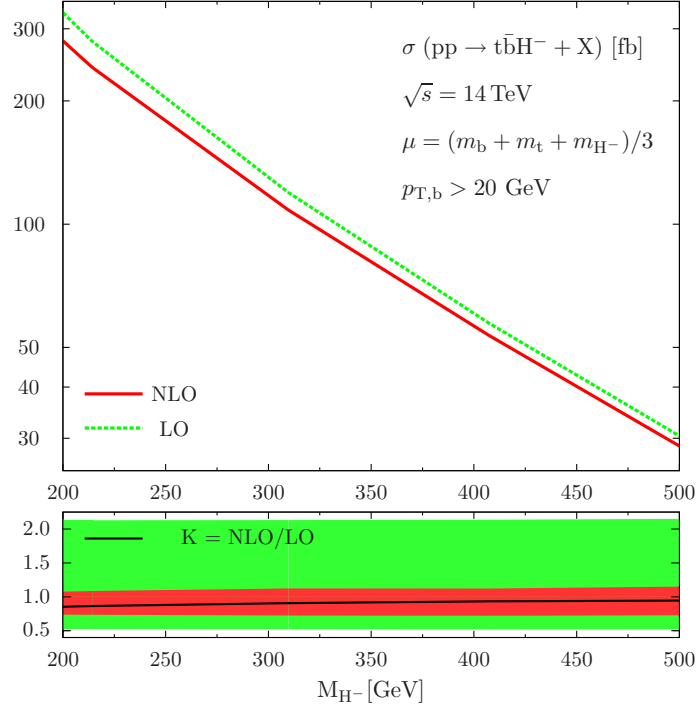
Figure 5: Total LO and NLO cross sections for pp → t b̄H⁻ + X at the LHC (14 TeV) as a function of the Higgs-boson mass, with a cut of $p_{\mathrm{T,b}} > 20$ GeV on the b-quark transverse momentum. The lower plots show the K-factor, $K = \sigma_{\mathrm{NLO}}/\sigma_{\mathrm{LO}}$, and the scale dependence of the LO and NLO cross section predictions for $\mu_0/3 < \mu < 3\mu_0$.
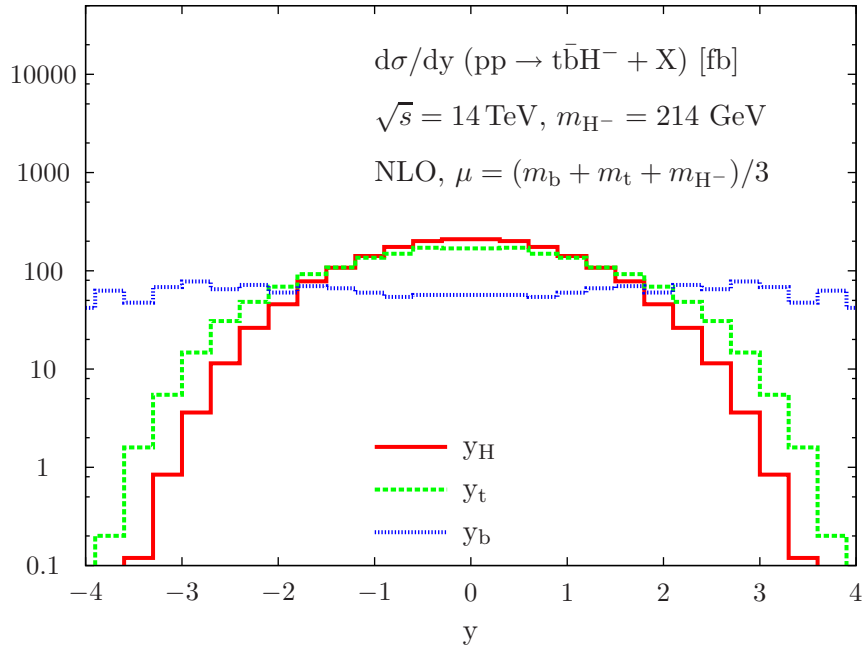
Figure 6: NLO transverse-momentum and rapidity distributions of the Higgs boson, the top quark, and the bottom quark for pp → tb̄H⁻ + X at the LHC (14 TeV).
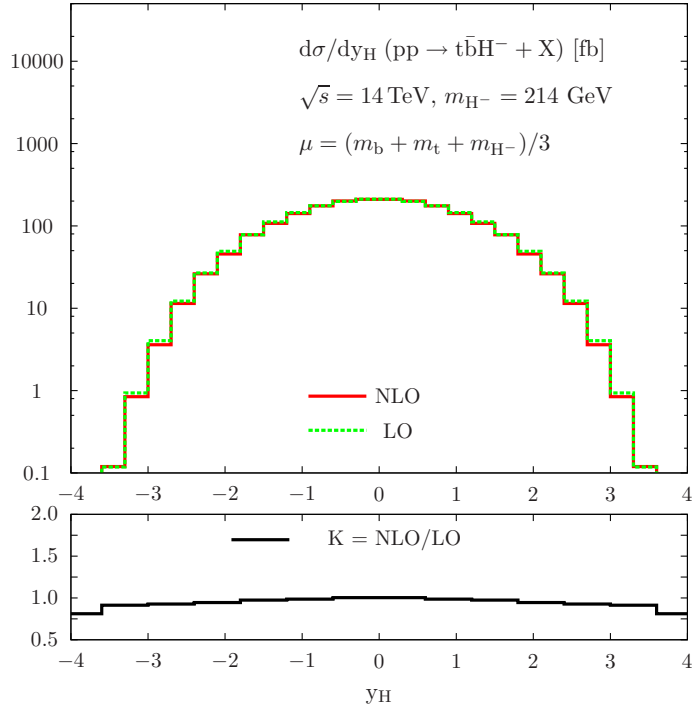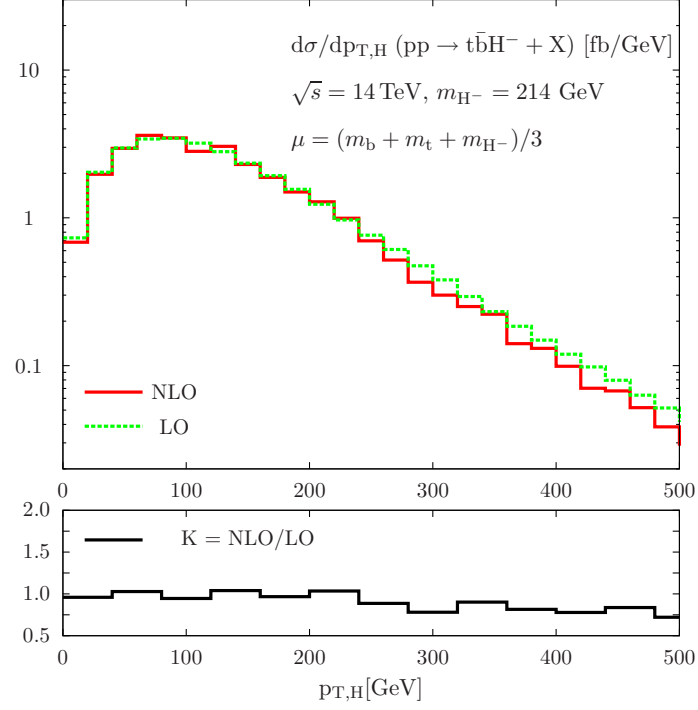
Figure 7: LO and NLO transverse-momentum and rapidity distributions of the Higgs boson for pp $\rightarrow$ t$\bar{\text{b}}$H$^-$ + X at the LHC (14 TeV). The lower plot shows the K-factor, K = $\sigma_{\text{NLO}}/\sigma_{\text{LO}}$.
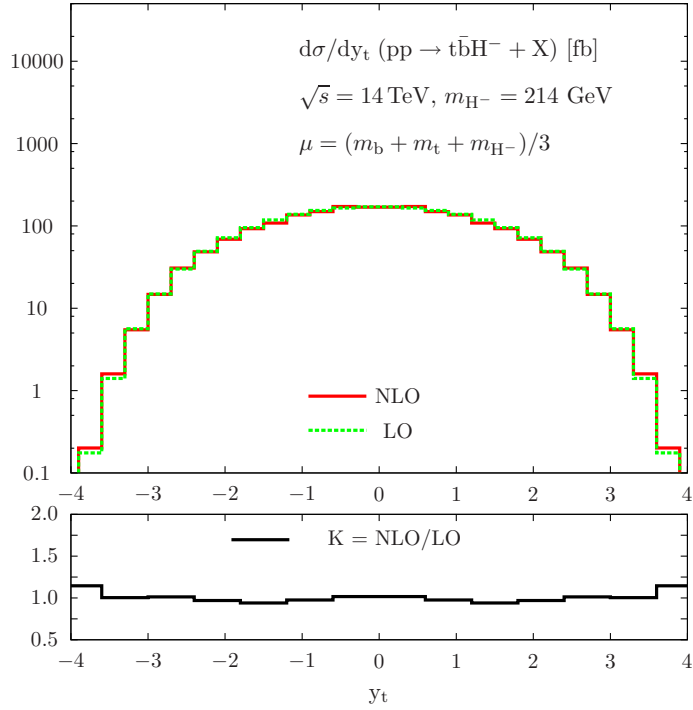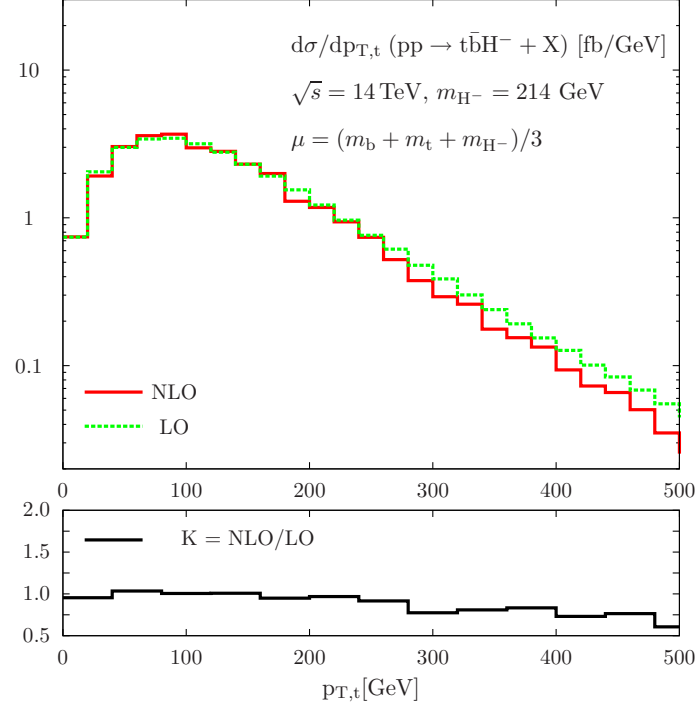
18

Figure 8: LO and NLO transverse-momentum and rapidity distributions of the top quark for pp → t$\bar{\text{b}}$H$^-$ + X at the LHC (14 TeV). The lower plot shows the K-factor, K = $\sigma_{\text{NLO}}/\sigma_{\text{LO}}$.
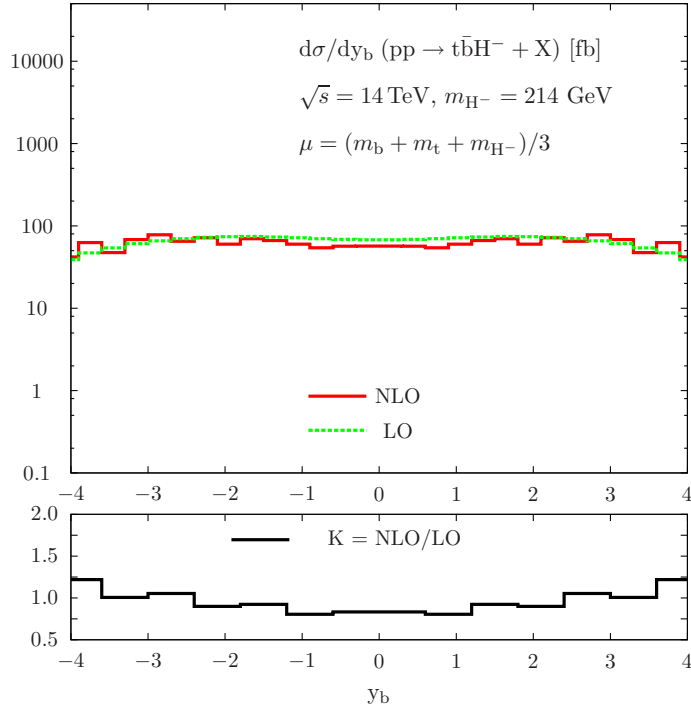
19
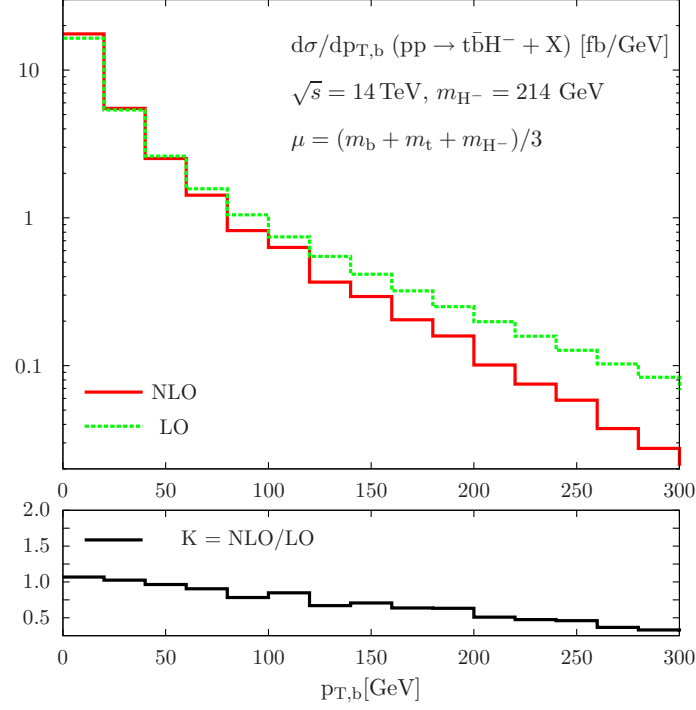
Figure 9: LO and NLO transverse-momentum and rapidity distributions of the bottom quark for pp → t̄bH⁻ + X at the LHC (14 TeV). The lower plot shows the K-factor, K = $\sigma_{\mathrm{NLO}}/\sigma_{\mathrm{LO}}$.
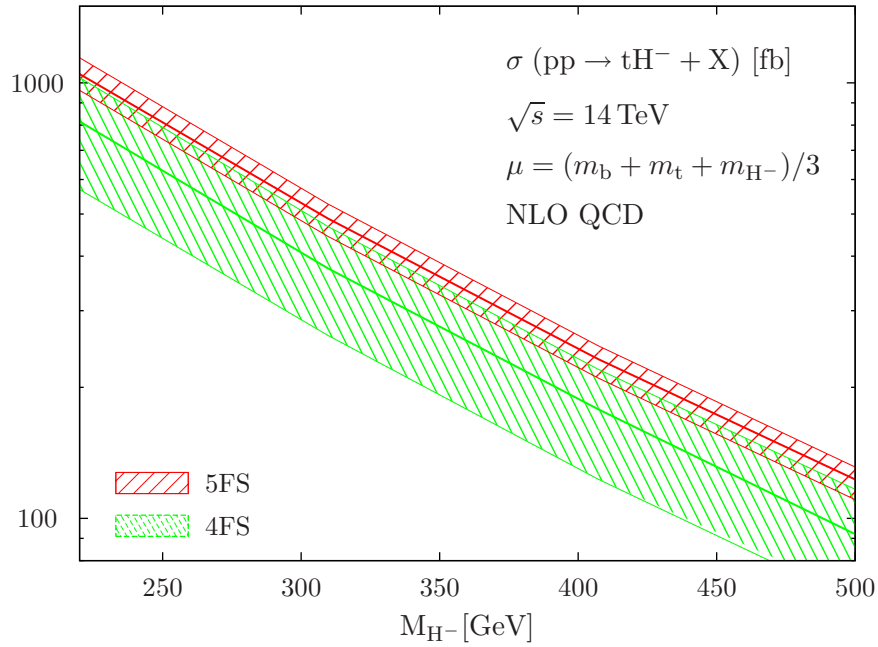
Figure 10: Total NLO cross section for pp $\rightarrow$ tH$^-$ + X at the LHC as a function of the Higgs-boson mass in the 4FS and the 5FS. Shown is the central prediction and the scale dependence for $\mu_0/3 < \mu < 3\mu_0$.
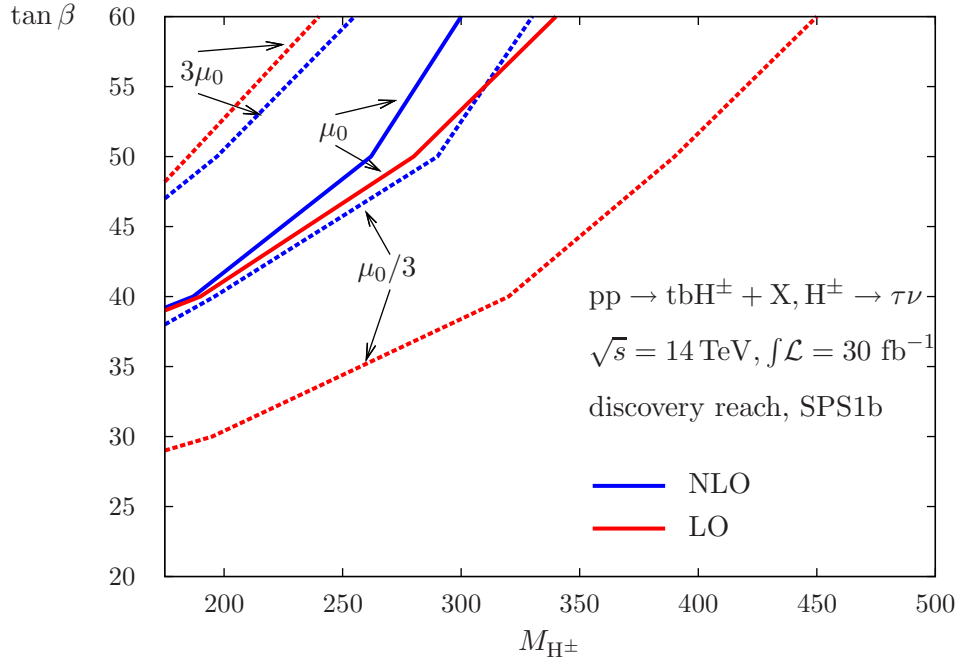
Figure 11: Discovery reach for MSSM charged Higgs bosons $H^{\pm}$, with $H^{\pm} \rightarrow \tau\nu$, at CMS [28] as a function of $\tan\beta$ and $M_{H^{\pm}}$. All other supersymmetric parameters have been fixed to the SPS 1b values. Higgs-boson discovery with $\int \mathcal{L} = 30$ fb^{-1} is possible in the areas above the curves. Shown are results based on the LO and NLO cross sections calculation in the 4FS with the central scale $\mu_0 = (m_{\mathrm{t}} + m_{\mathrm{b}} + M_{H^-})/3$ and scales set to $\mu = \mu_0/3$ and $3\mu_0$, respectively.

A SPS 1b benchmark scenario

For the SPS 1b benchmark [59] scenario discussed in this work we use the following input for $\tan\beta$, the supersymmetric Higgs mass parameter μ, the electroweak gaugino mass parameters $M_{1,2}$, the gluino mass $m_{\tilde{g}}$, the trilinear couplings $A_{\tau,\text{t,b}}$, the scale $\mu_R(\overline{\text{DR}})$ at which the $\overline{\text{DR}}$ input values are defined, the soft SUSY-breaking parameters in the diagonal entries of the squark and slepton mass matrices of the first and second generation M_{fi} (where $i = L, R$ refers to the left- and right-handed sfermions, $f = q, l$ to quarks and leptons, and $f = u, d, e$ to up and down quarks and electrons, respectively), and the analogous soft SUSY-breaking parameters for the third generation M_{fi}^{3G}:

$$
\begin{aligned}
\tan\beta &= 30.0 & M_{qL} &= 836.2 \text{ GeV} \\
\mu &= 495.6 \text{ GeV} & M_{dR} &= 803.9 \text{ GeV} \\
M_1 &= 162.8 \text{ GeV} & M_{uR} &= 807.5 \text{ GeV} \\
M_2 &= 310.9 \text{ GeV} & M_{lL} &= 334.0 \text{ GeV} \\
m_{\tilde{g}} &= 916.1 \text{ GeV} & M_{eR} &= 248.3 \text{ GeV} \\
A_\tau &= -195.8 \text{ GeV} & M_{qL}^{3G} &= 762.5 \text{ GeV} \\
A_\text{t} &= -729.3 \text{ GeV} & M_{dR}^{3G} &= 780.3 \text{ GeV} \\
A_\text{b} &= -987.4 \text{ GeV} & M_{uR}^{3G} &= 670.7 \text{ GeV} \\
\mu_R(\overline{\text{DR}}) &= 706.9 \text{ GeV} & M_{lL}^{3G} &= 323.8 \text{ GeV} \\
M_{eR}^{3G} &= 218.6 \text{ GeV}\,.
\end{aligned}
$$

The mass of the CP-odd Higgs boson M_A is varied and taken as input to calculate the charged-Higgs boson mass $M_{\text{H}^\pm}$, taking into account higher-order corrections up to two loops in the effective potential approach [60,61] as included in the program *HDECAY* [62].

References

[1] P. W. Higgs, Phys. Lett. **12**, 132 (1964); Phys. Rev. Lett. **13**, 508 (1964) and Phys. Rev. **145**, 1156 (1966); F. Englert and R. Brout, Phys. Rev. Lett. **13**, 321 (1964); G. S. Guralnik, C. R. Hagen and T. W. Kibble, Phys. Rev. Lett. **13**, 585 (1964).

[2] A. Heister *et al.* [ALEPH Collaboration], Phys. Lett. B **543** (2002) 1 [arXiv:hep-ex/0207054].

[3] J. F. Gunion and A. Turski, Phys. Rev. D **39** (1989) 2701.

[4] A. Brignole, Phys. Lett. B **277** (1992) 313.

[5] M. A. Diaz and H. E. Haber, Phys. Rev. D **45** (1992) 4246.

[6] M. Frank, T. Hahn, S. Heinemeyer, W. Hollik, H. Rzehak and G. Weiglein, JHEP **0702** (2007) 047 [arXiv:hep-ph/0611326].

[7] S. Schael *et al.* [ALEPH Collaboration], Eur. Phys. J. C **47** (2006) 547 [arXiv:hep-ex/0602042].

[8] A. Abulencia *et al.* [CDF Collaboration], Phys. Rev. Lett. **96** (2006) 042003 [arXiv:hep-ex/0510065].

[9] V. M. Abazov *et al.* [D0 Collaboration], Phys. Rev. Lett. **88** (2002) 151803 [arXiv:hep-ex/0102039].

[10] ATLAS: Detector and physics performance technical design report, CERN-LHCC-99-014.

[11] G. L. Bayatian *et al.* [CMS Collaboration], J. Phys. G **34** (2007) 995.

[12] A. Djouadi, Phys. Rept. **459** (2008) 1 [arXiv:hep-ph/0503173].

[13] S. Dittmaier, G. Hiller, T. Plehn and M. Spannowsky, Phys. Rev. D **77** (2008) 115001 [arXiv:0708.0940 [hep-ph]].

[14] R. M. Barnett, H. E. Haber and D. E. Soper, Nucl. Phys. B **306** (1988) 697; D. A. Dicus and S. Willenbrock, Phys. Rev. D **39** (1989) 751.

[15] S. Dittmaier, M. Krämer and M. Spira, Phys. Rev. D **70** (2004) 074010 [hep-ph/0309204].

[16] J. Campbell *et al.*, [hep-ph/0405302].

[17] S. Dawson, C. B. Jackson, L. Reina and D. Wackeroth, Mod. Phys. Lett. A **21** (2006) 89 [hep-ph/0508293].

[18] C. Buttar *et al.*, [hep-ph/0604120].

[19] S. h. Zhu, Phys. Rev. D **67** (2003) 075006 [arXiv:hep-ph/0112109].

[20] G. P. Gao, G. R. Lu, Z. H. Xiong and J. M. Yang, Phys. Rev. D **66** (2002) 015007 [arXiv:hep-ph/0202016].

[21] T. Plehn, Phys. Rev. D **67** (2003) 014018 [arXiv:hep-ph/0206121].

[22] E. L. Berger, T. Han, J. Jiang and T. Plehn, Phys. Rev. D **71** (2005) 115012 [arXiv:hep-ph/0312286].

[23] N. Kidonakis, PoS HEP2005 (2006) 336 [arXiv:hep-ph/0511235].

[24] W. Peng, M. Wen-Gan, Z. Ren-You, J. Yi, H. Liang and G. Lei, Phys. Rev. D **73** (2006) 015012 [arXiv:hep-ph/0601069].

[25] M. Beccaria, G. Macorini, L. Panizzi, F. M. Renard and C. Verzegnassi, Phys. Rev. D **80** (2009) 053011 [arXiv:0908.1332 [hep-ph]].

[26] N. Kidonakis, arXiv:1005.4451 [hep-ph].

[27] C. Weydert *et al.*, Eur. Phys. J. C **67** (2010) 617 [arXiv:0912.3430 [hep-ph]].

[28] R. Kinnunen, CMS NOTE-2006/100.

[29] J. L. Diaz-Cruz and O. A. Sampayo, Phys. Rev. D **50** (1994) 6820.

[30] F. Borzumati, J. L. Kneur and N. Polonsky, Phys. Rev. D **60** (1999) 115011 [arXiv:hep-ph/9905443].

[31] D. J. Miller, S. Moretti, D. P. Roy and W. J. Stirling, Phys. Rev. D **61** (2000) 055011 [arXiv:hep-ph/9906230].

[32] C. Amsler *et al.* [Particle Data Group], Phys. Lett. B **667** (2008) 1.

[33] W. Beenakker, S. Dittmaier, M. Krämer, B. Plümper, M. Spira and P. M. Zerwas, Phys. Rev. Lett. **87** (2001) 201805 [arXiv:hep-ph/0107081].

[34] W. Beenakker, S. Dittmaier, M. Krämer, B. Plümper, M. Spira and P. M. Zerwas, Nucl. Phys. B **653** (2003) 151 [arXiv:hep-ph/0211352].

[35] L. Reina, S. Dawson, D. Wackeroth, Phys. Rev. **D65** (2002) 053017 [hep-ph/0109066].

[36] S. Dawson, C. Jackson, L. H. Orr *et al.*, Phys. Rev. **D68** (2003) 034022 [hep-ph/0305087].

[37] Manuel Walser, "NLO QCD and SUSY-QCD corrections to associated MSSM Higgs production with heavy quarks at hadron colliders", disseration ETH Zürich NO. 17592, 2008

[38] J. Küblbeck, M. Böhm and A. Denner, Comput. Phys. Commun. **60** (1990) 165; H. Eck and J. Küblbeck, *Guide to FeynArts 1.0*, University of Würzburg, 1992.

[39] T. Hahn, Comput. Phys. Commun. **140** (2001) 418 [hep-ph/0012260].

[40] S. Dittmaier, Nucl. Phys. B **675** (2003) 447 [arXiv:hep-ph/0308246].

[41] A. Bredenstein, A. Denner, S. Dittmaier and S. Pozzorini, JHEP **0808** (2008) 108 [arXiv:0807.1248 [hep-ph]].

[42] A. Denner and S. Dittmaier, Nucl. Phys. B **658** (2003) 175 [hep-ph/0212259].

[43] G. Passarino and M. Veltman, Nucl. Phys. B **160** (1979) 151.

[44] A. Denner and S. Dittmaier, Nucl. Phys. B **734** (2006) 62 [arXiv:hep-ph/0509141].

[45] G. 't Hooft and M. Veltman, Nucl. Phys. B **153** (1979) 365;
W. Beenakker and A. Denner, Nucl. Phys. B **338** (1990) 349;
A. Denner, U. Nierste and R. Scharf, Nucl. Phys. B **367** (1991) 637.

[46] T. Hahn and M. Perez-Victoria, Comput. Phys. Commun. **118** (1999) 153 [arXiv:hep-ph/9807565]; G. J. van Oldenborgh, Comput. Phys. Commun. **66** (1991) 1.

[47] S. Catani and M. H. Seymour, Nucl. Phys. B **485** (1997) 291 [Erratum-ibid. B **510** (1998) 503] [arXiv:hep-ph/9605323];
S. Catani, S. Dittmaier, M. H. Seymour and Z. Trócsányi, Nucl. Phys. B **627** (2002) 189 [arXiv:hep-ph/0201036].

[48] J. Alwall *et al.*, JHEP **0709** (2007) 028 [arXiv:0706.2334 [hep-ph]].

[49] H. Murayama, I. Watanabe and K. Hagiwara, KEK-91-11, January 1992 (unpublished).

[50] E. Braaten and J. P. Leveille, Phys. Rev. D **22** (1980) 715;
M. Drees and K. I. Hikasa, Phys. Lett. B **240** (1990) 455 [Erratum-ibid. B **262** (1991) 497].

[51] L. J. Hall, R. Rattazzi and U. Sarid, Phys. Rev. D **50** (1994) 7048 [hep-ph/9306309].

[52] R. Hempfling, Phys. Rev. D **49** (1994) 6168.

[53] M. Carena, M. Olechowski, S. Pokorski and C. E. M. Wagner, Nucl. Phys. B **426** (1994) 269 [hep-ph/9402253].

[54] D. M. Pierce, J. A. Bagger, K. T. Matchev and R. J. Zhang, Nucl. Phys. B **491** (1997) 3 [hep-ph/9606211].

[55] M. Carena, D. Garcia, U. Nierste and C. E. M. Wagner, Nucl. Phys. B **577** (2000) 88 [hep-ph/9912516].

[56] J. Guasch, P. Häfliger and M. Spira, Phys. Rev. D **68** (2003) 115001 [hep-ph/0305101].

[57] See `https://twiki.cern.ch/twiki/bin/view/LHCPhysics/CrossSections`

[58] A. D. Martin, W. J. Stirling, R. S. Thorne and G. Watt, arXiv:1007.2624 [hep-ph].

[59] B. C. Allanach *et al.*, Eur. Phys. J. C **25** (2002) 113 [eConf **C010630** (2001) P125] [hep-ph/0202233].

[60] M. Carena, H.E. Haber, S. Heinemeyer, W. Hollik, C.E. Wagner and G. Weiglein, Nucl. Phys. **B580** (2000) 29.

[61] H. E. Haber, R. Hempfling and A. H. Hoang, Z. Phys. C **75** (1997) 539 [arXiv:hep-ph/9609331].

[62] A. Djouadi, J. Kalinowski and M. Spira, Comput. Phys. Commun. **108** (1998) 56 [arXiv:hep-ph/9704448]; A. Djoaudi, M. Mühlleitner, J. Kalinowski and M. Spira in J. M. Butterworth *et al.*, arXiv:1003.1643 [hep-ph].

[63] A. D. Martin, W. J. Stirling, R. S. Thorne and G. Watt, Eur. Phys. J. C **63** (2009) 189 [arXiv:0901.0002 [hep-ph]].

[64] D. Noth and M. Spira, Phys. Rev. Lett. **101** (2008) 181801 [arXiv:0808.0087 [hep-ph]].

[65] M. Glück, P. Jimenez-Delgado, E. Reya and C. Schuck, Phys. Lett. B **664** (2008) 133 [arXiv:0801.3618 [hep-ph]].

[66] S. Dittmaier, M. Krämer, A. Mück and T. Schlüter, JHEP **0703** (2007) 114 [arXiv:hep-ph/0611353].

[67] J. M. Campbell, R. Frederix, F. Maltoni and F. Tramontano, Phys. Rev. Lett. **102** (2009) 182003 [arXiv:0903.0005 [hep-ph]] and JHEP **0910** (2009) 042 [arXiv:0907.3933 [hep-ph]].

[68] A. D. Martin, R. G. Roberts, W. J. Stirling and R. S. Thorne, Phys. Lett. B **604** (2004) 61 [arXiv:hep-ph/0410230].

[69] M. Hashemi, S. Heinemeyer, R. Kinnunen, A. Nikitenko and G. Weiglein, arXiv:0804.1228 [hep-ph].

[70] A. Djouadi, M. M. Mühlleitner and M. Spira, Acta Phys. Polon. B **38** (2007) 635 [arXiv:hep-ph/0609292].